Three-Dimensional Dosimetry for Radioimmunotherapy Treatment Planning

George Sgouros, Stephen Chiu, Keith S. Pentlow, Linda J. Brewster, Hovanes Kalaigian, Bernard Baldwin, Farhad Daghighian, Martin C. Graham, Steven M. Larson and Radhe Mohan

Department of Medical Physics and Nuclear Medicine Service, Memorial Sloan-Kettering Cancer Center, New York, New York

Absorbed-dose calculations for radioimmunotherapy are generally based on tracer imaging studies of the labeled antibody. Such calculations yield estimates of the average dose to normal and target tissues assuming idealized geometries for both the radioactivity source volume and the target volume. This work describes a methodology that integrates functional information obtained from SPECT or PET with anatomical information from CT or MRI. These imaging modalities are used to define the actual shape and position of the radioactivity source volume relative to the patient's anatomy. This information is then used to calculate the spatially varying absorbed dose, depicted in "colorwash" superimposed on the anatomical imaging study. By accounting for individual uptake characteristics of a particular tumor and/or normal tissue volume and superimposing resulting absorbed-dose distribution over patient anatomy, this approach provides a patient-specific assessment of the target-to-surrounding normal tissue absorbed-dose ratio. Such information is particularly important in a treatment planning approach to radioimmunotherapy, wherein a therapeutic administration of antibody is preceded by a tracer imaging study to assess therapeutic benefit.

J Nucl Med 1993; 34:1595–1601

Calculation of the absorbed dose to normal and target tissues for radioimmunotherapy presents several challenges not encountered in traditional internally administered radionuclide absorbed dose calculations. Since most internally administered agents are used for imaging and diagnosis, the absorbed dose to critical organs is usually far below the level associated with tissue damage. Those cases in which radionuclides are used for therapy (e.g., radioiodine therapy of thyroid disease) exhibit a high target-to-normal tissue activity concentration ratio. This contrasts with radioimmunotherapy in which the high levels of administered activity and the biodistribution of labeled antibody may lead to normal tissue morbidity.

A key obstacle to meeting the more stringent demands on the accuracy of absorbed dose calculations for radiolabeled antibody therapy has been the difficulty associated with obtaining accurate, patient-specific biodistribution data. Using PET imaging of antibodies labeled with positron emitters (*1–4*), and quantitative imaging with single photon emission computed tomography (SPECT) (*5–9*), this difficulty may be overcome.

A secondary and related obstacle is the difficulty of performing absorbed dose calculations, given the detailed biodistribution information described above. The most prevalent approach to internal radionuclide dosimetry, the S-factor based methodology (*10–12*) developed by the Medical Internal Radiation Dose (MIRD) Committee, cannot accommodate all of the information provided by PET and SPECT imaging. Specifically, information regarding the shape and position of the activity volume is not included, since the S-factors (mean dose per unit cumulated activity) were calculated assuming idealized or "Reference Man" organ geometries (*11*). The source volume or volumes of radioactivity, therefore, always correspond to fixed organ geometries. This limitation is particularly troublesome in radioimmunotherapy calculations since it precludes calculation of the dose to normal tissues arising from activity in a tumor.

Several approaches to the solution of this problem have been implemented. The simplest of these assumes that activity in the tumor may be assigned to some proximal organ volume (i.e., an organ containing or adjacent to the tumor) for which S-factors have been calculated. The dose to normal tissues is then obtained by replacing the proximal organ for the tumor as the source of radioactivity in the calculation (*13*). This approach is usually adequate in calculating the absorbed dose to a tissue that is far from the tumor; it is not useful for calculating the dose to a tissue containing or adjacent to the tumor. A more rigorous but also computationally more demanding approach, in which the Reference Man geometry is modified to include a spherical tumor, involves an "on-the-fly" Monte Carlo calculation (*14*). Dose calculation techniques which do not rely on S-factors generally assume idealized geometries for both tumor and normal tissue activity distributions (*15–17*).

This paper presents a technique for performing three-dimensional internal dosimetry treatment planning (*18*)

Received Sept. 30, 1992; revision accepted May 11, 1993.

For correspondence or reprints contact: George Sgouros, PhD, Dept. of Medical Physics, Memorial Sloan-Kettering Cancer Center, 1275 York Ave., New York NY 10021.

which integrates three-dimensional information regarding the activity distribution from PET or SPECT imaging with anatomical information from MR or CT imaging. Absorbed dose calculations for two patients imaged with PET using ^{124}I-labeled 3F8 antibody are presented. Two dosimetry calculations were performed for each patient, assuming a therapeutic infusion of antibody labeled with ^{131}I or with ^{125}I. Details regarding PET imaging with ^{124}I and activity quantitation of ^{124}I-labeled 3F8 antibody in these patients have been published previously (*1,3,4*).

METHODS

Patient Imaging

Characteristics of 3F8 antibody, as well as its labeling with a short-lived positron emitter, have been reported previously (*19–21*). Details regarding patient attributes and ^{124}I imaging and quantitation using PET have also been reported previously (*3,4*). PET images from two patients are used to illustrate the dose calculation methodology. The first patient (Patient 1) suffered from neuroblastoma and exhibited a large tumor mass in the retroperitoneum; she underwent CT imaging (GE 9800, GE Medical Systems, Milwaukee, WI) in addition to the PET imaging (PC4600, Cyclotron Corp., Berkeley, CA). The second patient (Patient 2) exhibited bilateral glioblastoma multiforme. In addition to PET imaging, this patient also underwent magnetic resonance imaging (MRI) (SIGNA 1.5T, GE Medical Systems, Milwaukee, WI).

Delineation of Activity Source Volume

The expected distribution of a therapeutic administration of ^{131}I or ^{125}I-labeled 3F8 was obtained from the measured biodistribution of ^{124}I-labeled 3F8 antibody obtained from the tracer PET imaging studies. Three-dimensional representations of the activity containing volumes were generated for each patient by drawing a contour around the periphery of each activity region as seen on each of several contiguous PET slices. This was accomplished by converting PET images into an image format readable by the previously described Internal Dosimetry for Treatment Planning (IDTP) software package (*18*). This package uses the support structure (i.e., image display and handling, region of interest definition, etc.) of an external beam, three-dimensional treatment planning program developed at the Medical Physics Department of Memorial Sloan-Kettering Cancer Center (*22*).

Image Registration

The PET contours, representing activity distribution, were registered with the anatomical imaging modalities, MRI or CT, by superimposing the contours for a given PET slice on the corresponding MRI or CT slice. Slice interpolation was not performed to generate the appropriate MRI or CT slice for a given PET slice. Rather, the slice corresponding to the nearest z-value was used. Once the contours were superimposed onto the appropriate MRI or CT image slice, the user manually adjusted the PET contours with a trackball to rotate, translate, expand or contract them to provide an approximate match to the anatomical image information. The user-specified transformation was then applied to the contours on the remaining PET slices. Contour manipulations were performed using software developed as part of the external beam treatment planning package (*22*).

It is important to note that the dose calculation technique herein described does not require that the image registration be performed as described above. If the functional images have already been registered to the anatomical imaging study, the activity contours drawn on these images can then be transposed directly to the anatomical imaging study. This allows for the use of more sophisticated image registration techniques (*23–30*).

Absorbed Dose Calculations

Dose calculations were performed for ^{131}I and for ^{125}I. Each activity source volume, drawn from the PET images, was assigned a single cumulated activity concentration value of 10^6 MBq-sec/cm^3 (i.e., within each source volume a uniform distribution of activity was assumed). During display of the absorbed dose distribution, the cumulated activity concentration may be scaled to match the actual value obtained for each region. Assignment of cumulated activity concentration to each activity source volume implicitly assumes that the spatial activity distribution at a given time represents a good approximation to the spatial cumulated activity distribution (i.e., the integral of the spatial activity distribution over time). Details regarding the dose calculation procedure have been described previously (*18*). The method requires a previously generated point-source kernel (i.e., table of absorbed dose as a function of distance from a point-source emitter) for each radionuclide, a collection of contours comprising one or more activity source volumes and a target plane (generally chosen to intersect a therapy-limiting or target tissue). The algorithm convolves the three-dimensional cumulated activity distribution (as defined by the activity source volumes) with the point source kernel to yield a two-dimensional matrix of dose values corresponding to points on the target plane. The dose matrix is converted to a colorwash or isodose contour display which is overlaid on the target CT or MR image slice. The point source kernels for ^{131}I and ^{125}I used in these calculations were generated using the Electron Gamma Shower (EGS) Monte Carlo simulation program (*31*), assuming an isotropic water-equivalent medium (*18*). Point kernels from other sources could also be used. To reduce the Monte Carlo simulation time, only photon emissions were included in the simulations for both ^{131}I and ^{125}I. Due to their short range, the electron emissions contribute to the local dose only and may be added to the source tissue absorbed dose by assuming local deposition (*12*). In contrast to the previously published description of this dose calculation methodology (*18*), the collection of contours used to depict the activity source volume were generated from the actual activity distribution obtained from PET imaging rather than from CT-based anatomical information.

Display of Activity Source Volumes

Once the individual contours comprising the activity source volumes are generated, they may be displayed in a three-dimensional "wire-frame" diagram along with contours representing anatomical information obtained from MRI or CT. Such a display is useful in depicting the geometric relationship between the activity distribution and patient anatomy. In particular, regions of low activity uptake due to tumor necrosis or due to inhomogeneities of antigen expression may be visualized in relation to the anatomy.

Display of Absorbed Dose Distribution

The final output of the absorbed dose calculation program is a two-dimensional matrix of dose values corresponding to points on the target plane. One such matrix is generated for each activity source volume. The dose values are displayed in colorwash superimposed over the target plane. The dose to the target plane arising from each source volume (i.e., each dose matrix) may be individually displayed and scaled. By scaling the dose from each

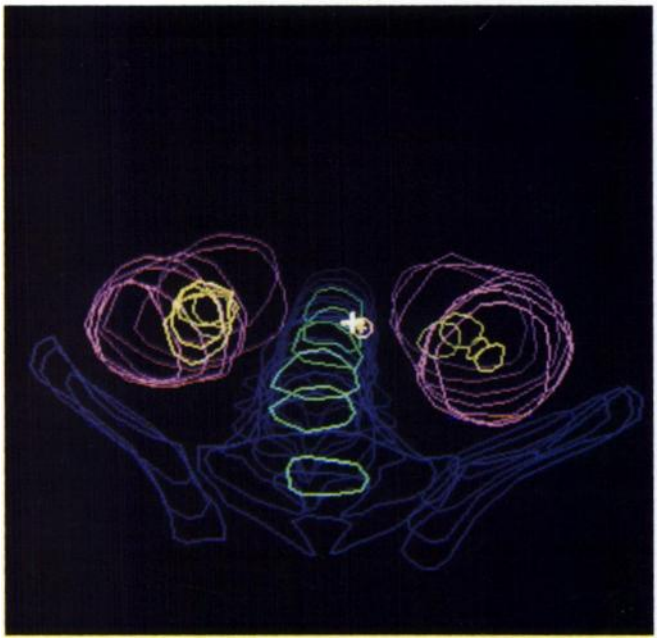

FIGURE 1. A transverse view, observed from inferior and slightly above coronal midplane, of a wire-frame diagram showing: bones of pelvis and spinal column in dark blue; marrow space within each vertebral body in light green; and kidneys in pink. Each was delineated by drawing contours on CT-slice images. Yellow contours represent activity in kidneys delineated from PET-slice images.

source volume according to that volume's cumulated activity concentration and "turning on" all of the dose matrices, a colorwash display may be generated that represents the total dose to the target plane from all of the delineated sources of activity. By allowing the user to selectively turn on or off dose contributions from individual source volumes, the system permits determination of the relative dose contribution to a given region from each individual activity source volume. This same approach may also be used to determine the effect of a dual isotope injection. By turning on the absorbed dose matrices corresponding to both ^{131}I and to ^{125}I, for example, one may assess the effect on the absorbed dose distribution of the combined emissions.

RESULTS

Figure 1 depicts the three-dimensional wire-frame representation for Patient 1. To better depict the activity-containing structures, the CT contours corresponding to the large tumor mass are not shown since the tumor was not visualized by PET; the tumor did not take up the labeled antibody. Activity was observed in the kidneys and in the marrow. Comparing the contours representing PET activity in the kidneys (in yellow) with the anatomical definition of the kidneys from CT (in purple), one may observe that the activity was largely confined to the collecting tubules of the kidneys and may represent excretion of free iodide. This example illustrates the advantages both of incorporating functional imaging information to determine the absorbed dose and also of calculating the spatial variation in absorbed dose. A traditional S-Factor-based calculation of the absorbed dose to kidneys from activity within the kidneys would require the assumption that the cumulated activity obtained from PET be uniformly distributed throughout the whole volume of the kidneys and would provide an estimate of the average absorbed dose over the kidneys. Figures 2A and 2B depict the absorbed dose distribution for ^{131}I and ^{125}I photon emissions, respectively. In both cases the maximum absorbed dose occurs at the center of the kidneys and falls off so that approximately 25% and 12% of the maximum dose is achieved at the kidney periphery for ^{131}I and ^{125}I, respectively.

The more rapid drop in dose away from the source of activity for ^{125}I is due to this radionuclide's lower energy photon emissions. Figures 2A and 2B also depict the effect of marrow activity on the absorbed dose distribution. Both figures show that the spinal column, a possible dose-limit-

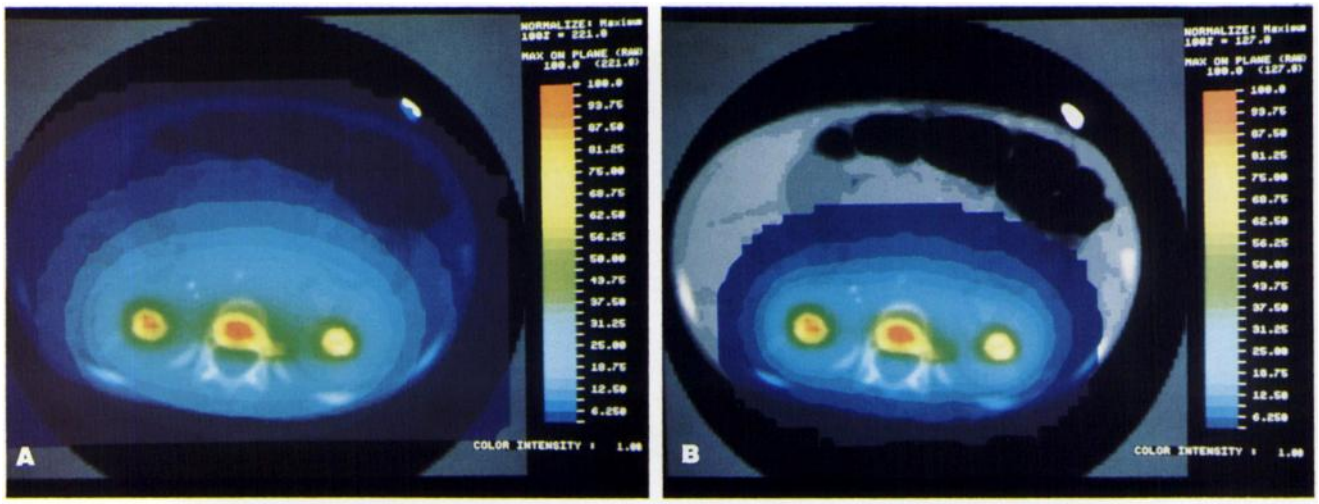

FIGURE 2. A colorwash display, superimposed on CT image of Patient 1, depicting spatial distribution of absorbed dose arising from activity in marrow and kidneys, delineated using PET images. A cumulated activity concentration of 10^6 MBq-sec/cm^3 was assigned to each activity-source volume. Maximum absorbed dose (cGy) is shown on upper right. (A) ^{131}I photon emissions. (B) ^{125}I photon emissions.

FIGURE 3.
A transverse view, observed from superior and slightly to left of sagittal midplane, of a wire frame diagram showing: brain in green; eyes in blue and yellow; an egg-shaped tumor in the right hemisphere in yellow (designated Tumor 1); and an irregularly shaped tumor in the left hemisphere in blue (designated Tumor 2). Each of these structures was delineated using MRI images. Also shown are contours corresponding to distribution of activity in Tumor 1 (pink) and Tumor 2 (orange), delineated using PET.

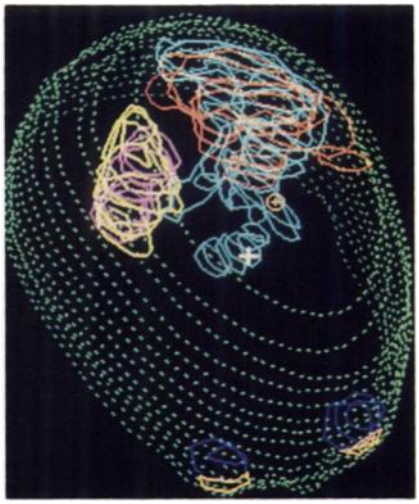

ing organ after the red marrow, receives approximately 31%–37% of the maximum absorbed dose.

The wire-frame diagram for Patient 2 is depicted in Figure 3. MRI delineation of the smaller, egg-shaped tumor to the patient's right (Tumor 1, in yellow) is shown to coincide well with the corresponding volume of activity as determined from PET (shown in pink). In contrast, the large, irregularly shaped tumor (Tumor 2) to the patient's left is shown to extend (in blue) beyond the region of activity uptake (in orange). At the periphery, the region of activity extends beyond the boundaries of the tumor as determined by MRI. Figures 4A and 4B depict the absorbed dose distribution arising for ^{131}I and for ^{125}I photons, respectively, from the activity volumes shown in Figure 3. Since the MRI slice selected corresponds to a PET slice in which activity is not observed in Tumor 2, the maximum absorbed dose occurs near the center of Tumor 1 for both ^{131}I and for ^{125}I. At this level, approximately 60% of the maximum dose is achieved in Tumor 2 for ^{131}I photons and approximately 50% for ^{125}I photons. In both cases, the effect of radioactivity in slices above and below the one

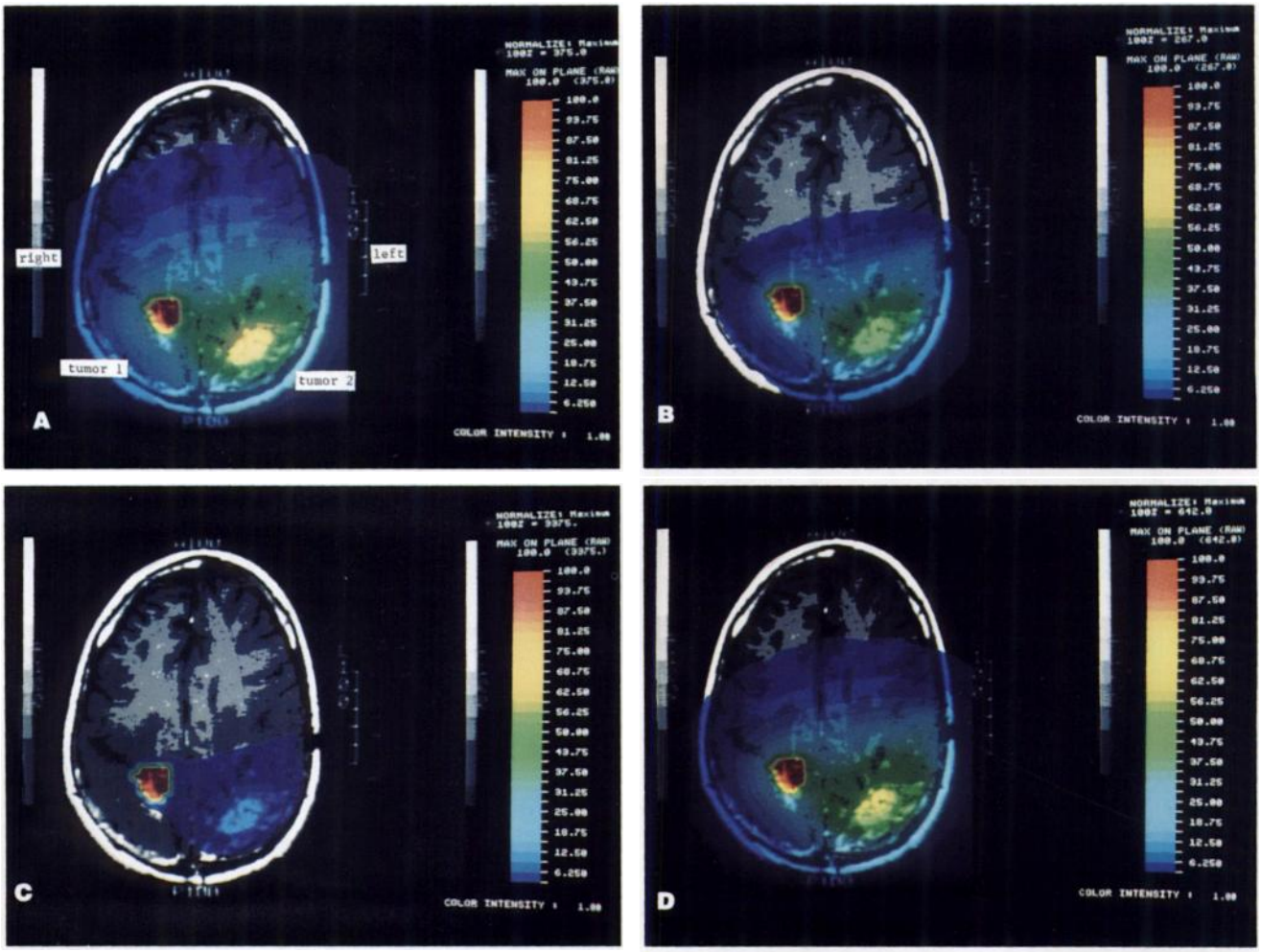

FIGURE 4. A colorwash display, superimposed on an MRI image of Patient 2, depicting spatial distribution of absorbed dose due to activity in Tumor 1 (on left) and Tumor 2 (on right), delineated using PET images. A cumulated activity concentration of 10^6 MBq-sec/m^3 was assigned to both tumor activity volumes. (A) ^{131}I photon emissions, (B) ^{125}I photon emissions, (C) total ^{131}I emissions (electron and photon) and (D) both ^{131}I and ^{125}I photon emissions.

selected is shown by the green "halo" around Tumor 2. The differences in the dose distribution between ^{131}I and ^{125}I illustrate several important concepts. Tumor 2 in the ^{131}I dose distribution achieves a significantly greater dose relative to the maximum than is achieved with ^{125}I. This demonstrates the compensatory effect of longer range emissions for regions that do not exhibit uniform uptake of radioactivity. On the other hand, as seen by the extent of the dark blue shading, the drop-off in absorbed dose for ^{125}I is much more rapid than that for ^{131}I; given uniform uptake of radioactivity within the tumor and minimal uptake in normal tissues, ^{125}I photon emissions would yield a greater tumor to normal tissue ratio. The total absorbed dose from both photon and electron emissions for ^{131}I is shown in Figure 4C. Since the electron contribution to the absorbed dose is much higher than the photon contribution, most of the photon dose information is below the colorscale of the image. The total ^{131}I absorbed dose to Tumor 2, which did not exhibit activity uptake at this level, is approximately 6% of the maximum dose or approximately 200 cGy. As seen on Figure 4A, this dose arises from photon emissions only. A compromise between the compensatory effect of ^{131}I and the normal tissue sparing of ^{125}I photons may be arrived at by co-injecting ^{131}I and ^{125}I-labeled antibody. Figure 4D depicts the absorbed dose distribution from both ^{131}I and ^{125}I photons. The absorbed dose to Tumor 2 relative to the maximum is between that observed for ^{131}I and ^{125}I, as is the extent of normal tissue dose as seen by the dark blue shading.

DISCUSSION

Using quantitative imaging of radiolabeled antibody with SPECT (*5–9*) and more recently with PET (*1–4*), it is now possible to obtain detailed information regarding the spatial distribution of administered antibody. Validation studies using surgical specimens to verify radioactivity concentration measurements performed with quantitative imaging have demonstrated good agreement for ^{131}I (*32*). In a radioimmunotherapy treatment planning context, such tracer-imaging information is used to evaluate patient benefit prior to a therapeutic administration of labeled antibody (*18,33,34*). The methodology herein presented for incorporating the three-dimensional distribution of activity to calculate the spatially varying absorbed dose provides an additional tool in the treatment planning process. Unlike the traditional approach to organ dosimetry (*10–12*), patient variations in tumor and normal tissue anatomy as well as in radiolabeled antibody distribution are specifically taken into account in arriving at a spatial distribution of absorbed dose.

It is important to point out that, although a good approximation in most cases, caution is required in taking a biodistribution based upon a tracer dose of labeled antibody and applying it to a therapeutic administration of antibody, even if the milligram amount of antibody is kept constant. Three things could lead to an altered biodistribution of the labeled antibody: (1) increased radiolabel loss due to higher specific activity; (2) tumor cell kill; or (3) normal tissue morbidity (*35*).

Since the radioactivity distribution is defined using PET or SPECT imaging, it is also important to note that the absorbed dose calculations are subject to the uncertainties associated with image quantitation using these modalities (*36–42*). This concern is also present in conventional S-factor-based dosimetry in which estimates of organ radioactivity are obtained from nuclear medicine imaging. In both cases, the loss in counts associated with image attenuation and the artifactual increase in counts associated with Compton scatter of photons need to be addressed. These concerns are particularly important for SPECT quantitation and their severity will depend upon the radionuclide, the inhomogeneity in anatomical density, the spatial distribution of activity and the acquisition and camera characteristics (i.e., reconstruction algorithm, collimator type, number of detector heads, etc.) (*40–42*). Although still important, these concerns are diminished for PET since the characteristics of positron decay allow for coincidence detection of the counts. Attenuation and accidental coincidence corrections are still necessary and will depend upon the anatomical density, the spatial distribution of activity and the acquisition parameters and camera characteristics (*36–39*). Both the functional and anatomical imaging modalities are subject to partial volume effects. These need to be considered, especially with regard to their impact on the accuracy of image registration. The errors associated with the three-dimensional dose calculation algorithm have been described previously (*18*).

Results depicted in Figures 2A, 2B, 4A, 4B and 4D correspond to the absorbed dose arising from photon emissions only. Figure 4C depicts the dose arising from both photon and electron emissions. Dose contribution from electron emissions may simply be obtained by multiplying the cumulated activity concentration within the activity volume by the equilibrium dose constant for electron emissions (*43*). This approach yields the average absorbed dose due to electrons; enhancement of biologic effect due to cellular or subcellular localization of the antibody or label is not accounted for by this method. To obtain the total absorbed dose, the dose from regions outside the immediate calculational volume, would also have to be added. The dose contributions from distant organs may be obtained using the standard S-factor formalism as described by the MIRD Committee (*10–12*); the dose to tumor from distant organs may be obtained using modifications of the S-factor formalism (*13,14*).

A key assumption in arriving at the dose distributions depicted in the figures is that the spatial distribution of activity at a given time represents a good approximation to the spatial distribution of the activity integral over time (i.e., the cumulated radioactivity). By performing time-

sequential PET or SPECT studies following a trace-labeled administration of antibody, changes in the spatial distribution of radioactivity may be followed. Ideally a collection of such images could be registered and then integrated, voxel-by-voxel, over time to yield a true parametric image of the cumulated radioactivity. In practice, this may be difficult because of the large uncertainty associated with quantitating the radioactivity within a very small volume (i.e., the voxel) (*6,9*). To minimize this problem, the average activity within a collection of sub-volumes, each containing an appropriate number of voxels, may have to be integrated.

The clinical implementability of a three-dimensional internal dosimetry approach for radioimmunotherapy treatment planning will depend to a significant extent on the time required to perform such calculations. Using a Digital Equipment Corporation Vaxstation 4000 computer workstation (Maynard, MA), the time required to obtain the absorbed dose distribution for each patient (the most computer-intensive task) was approximately 1 hr. No user interaction is required during this time. Prior to this step, however, the user must delineate the radioactivity distribution by drawing contours on a series of SPECT or PET slices. This is a user-intensive step that may take several hours to complete. The amount of time required to register the functional images (SPECT or PET) with the anatomical image set (MRI or CT) will depend upon the methodology used. The simple, contour-alignment approach that was used herein required approximately 15 min for each patient.

The approach to dosimetry and three-dimensional treatment planning that has been developed for external beam radiotherapy provides a useful paradigm upon which to model radioimmunotherapy treatment planning as it relates to absorbed dose calculations. Many of the support functions (image display and manipulation, region of interest and contour delineation, etc.) required in a three-dimensional internal radionuclide dosimetry package have already been developed for external beam treatment planning. By maintaining compatibility with an external beam package, the spatial distribution of absorbed dose arising from a combination of external beam radiotherapy and radioimmunotherapy could be easily integrated.

ACKNOWLEDGMENTS

The authors thank Drs. Ehud Arbit, Nai-Kong Cheung, Gene DiResta, Ronald Finn, Homer Macapinlac, Richard Lambrecht and Samuel Yeh for bringing about the original PET studies that were used as illustrative examples of the three-dimensional dose calculation methodology. George Sgouros is the recipient of a Cancer Research Institute/Jesselson Foundation Fellowship. This work was supported, in part, by DOE Grant DE-FG02-86ER60407 and NIH Grant U01-CA58260-01.

REFERENCES

1. Pentlow KS, Graham MC, Lambrecht RM, Cheung N-KV, Larson SM. Quantitative imaging of I-124 using positron emission tomography with applications to radioimmunodiagnosis and radioimmunotherapy. *Med Phys* 1991;18:357–366.
2. Wilson CB, Snook DE, Dhokia B, et al. Quantitative measurement of monoclonal antibody distribution and blood flow using positron emission tomography and iodine-124 in patients with breast cancer. *Int J Cancer* 1991;47:344–347.
3. Larson SM, Pentlow KS, Volkow ND, et al. PET scanning of iodine-124 as an approach to tumor dosimetry during treatment planning for radioimmunotherapy in a child with neuroblastoma. *J Nucl Med* 1992;33:2020–2023.
4. Daghighian F, Pentlow KS, Larson SM, et al. In vivo measurement of kinetics of radiolabeled monoclonal antibody in human tumor and applications to microdosimetry: PET studies of I-124-labeled 3F8 Mab in glioma. *Eur J Nucl Med* 1993:20:402–409.
5. DeNardo GL, Macey DJ, DeNardo SJ, Zhang CG, Custer TR. Quantitative SPECT of uptake of monoclonal antibodies. *Semin Nucl Med* 1989;19:22–32.
6. Zanzonico PB, Bigler RE, Sgouros G, Strauss A. Quantitative SPECT in radiation dosimetry. *Semin Nucl Med* 1989;19:47–61.
7. Israel O, Iosilevsky G, Front D, et al. SPECT quantitation of iodine-131 concentration in phantoms and human tumors. *J Nucl Med* 1990;31:1945–1949.
8. Leichner PK, Vriesendorp HM, Hawkins WG, et al. Quantitative SPECT for indium-111-labeled antibodies in the livers of beagle dogs. *J Nucl Med* 1991;32:1442–1444.
9. King MA, Long DT, Brill AB. SPECT volume quantitation: influence of spatial resolution, source size and shape, and voxel size. *Med Phys* 1991; 18:1016–1024.
10. Snyder WS, Ford MR, Warner GG, Watson SB. *"S," absorbed dose per unit cumulated activity for selected radionuclides and organs. MIRD Pamphlet No. 11, Revised.* New York, NY: Society of Nuclear Medicine; 1975.
11. Snyder WS, Ford MR, Warner GG. *Estimates of specific absorbed fractions for photon sources uniformly distributed in various organs of a heterogeneous phantom. MIRD Pamphlet No. 5, Revised.* New York, NY: Society of Nuclear Medicine; 1976.
12. Loevinger R, Budinger TF, Watson EE. *MIRD primer for absorbed dose calculations.* New York: The Society of Nuclear Medicine, 1989.
13. Sgouros G, Bigler RE, Zanzonico PB. DOSCAL: a tumor-incorporating mean absorbed dose calculation program [Abstract]. *J Nucl Med* 1988;29: 874.
14. Johnson TK. MABDOS: a generalized program for internal radionuclide dosimetry. *Computer Methods Programs Biomed* 1988;27:159–167.
15. Roeske JC, Chen GTY, Atcher RW, et al. Modeling of dose to tumor and normal tissue from intraperitoneal radioimmunotherapy with alpha and beta emitters. *Int J Radiat Oncol Biol Phys* 1990;19:1539–1548.
16. Sgouros G. Plasmapheresis in radioimmunotherapy of micrometastases: a mathematical modeling and dosimetrical analysis. *J Nucl Med* 1993;33: 2167–2179.
17. Fujimori K, Fisher DR, Weinstein JN. Integrated microscopic-macroscopic pharmacology of monoclonal antibody radioconjugates: the radiation dose distribution. *Cancer Res* 1991;51:4821–4827.
18. Sgouros G, Barest G, Thekkumthala J, et al. Treatment planning for internal radionuclide therapy: three-dimensional dosimetry for nonuniformly distributed radionuclides. *J Nucl Med* 1990;31:1884–1891.
19. Cheung NV, Saarinen UM, Neely JE, et al. Monoclonal antibodies to a glycolipid antigen on human neuroblastoma cells. *Cancer Res* 1985;45:2642–2649.
20. Miraldi FD, Nelson AD, Kraly C, et al. Diagnostic imaging of human neuroblastoma with radiolabeled antibody. *Radiology* 1986;161:413–418.
21. Finn RD, Cheung NV, Divgi CR, et al. Technical challenges associated with the radiolabeling of monoclonal antibodies utilizing short-lived, positron emitting radionuclides. *Nucl Med Biol* 1991;18:9–13.
22. Mohan R, Barest G, Brewster LJ, et al. A comprehensive three-dimensional treatment planning system. *Int J Radiat Oncol Biol Phys* 1988;15:481–495.
23. Schad LR, Boesecke R, Schlegel W, et al. Three-dimensional image correlation of CT, MR and PET studies in radiotherapy treatment planning of brain tumors. *J Comput Assist Tomogr* 1987;11:948–954.
24. Chen GTY, Pelizzari CA. Image correlation techniques in radiation therapy treatment planning. *Comput Med Imag Graph* 1989;13:235–240.
25. Kramer EL, Noz ME, Sanger SJ, Megibow AJ, Maguire GQ. CT-SPECT fusion to correlate radiolabeled monoclonal antibody uptake with abdominal CT findings. *Radiology* 1989;172:861–865.
26. Vogl G, Schwer C, Jauch M, et al. A simple superimposition method for anatomical adjustments of CT and SPECT images. *J Comp Assist Tomogr* 1989;13:929–931.

27. Pietrzyk U, Herholz K, Heiss W. Three-dimensional alignment of functional and morphological tomograms. *J Comp Assist Tomogr* 1990;14:51–59.
28. Alpert NM, Bradshaw JF, Correia JA. The principal axes transformation—a method for image registration. *J Nucl Med* 1990;31:1717–1722.
29. Kessler ML, Pitluck S, Petti P, Castro JR. Integration of multimodality imaging data for radiotherapy treatment planning. *Int J Radiat Oncol Biol Phys* 1991;21:1653–1667.
30. Holupka EJ, Kooy HM. A geometric algorithm for medical image correlations. *Med Phys* 1992;19:433–438.
31. Ford RL, Nelson WR. The EGS code system. *Stanford linear accelerator center report. No. 210*. Stanford, California: SLAC; 1978.
32. Erdi AK, Wessels BW, DeJager R, et al. Tumor activity confirmation and isodose curve display for patients receiving iodine-131—16.88 human monoclonal antibody [Abstract]. *Antibody Immunocon Radiopharm* 1992;5:355.
33. DeNardo GL, Raventos A, Hines HH, et al. Requirements for a treatment planning system for radioimmunotherapy. *Int J Radiat Oncol Biol Phys* 1985;11:335–348.
34. Eary JF, Press OW, Badger CC, et al. Imaging and treatment of B-cell lymphoma. *J Nucl Med* 1990;31:1257–1268.
35. Badger CC, Davis J, Nourigat C, et al. Biodistribution and dosimetry following infusion of antibodies labeled with large amounts of ^{131}I. *Cancer Res* 1991;51:5921–5928.
36. Hoffman EJ, Huang S, Phelps ME. Quantitation in positron emission computed tomography: 1. Effect of object size. *J Comput Assist Tomogr* 1979; 3:299–308.
37. Huang S, Hoffman EJ, Phelps ME, Kuhl DE. Quantitation in positron emission computed tomography: 2. Effects of inaccurate attenuation correction. *J Comput Assist Tomogr* 1979;3:804–814.
38. Huang S, Hoffman EJ, Phelps ME, Kuhl DE. Quantitation in positron emission computed tomography: 3. Effect of sampling. *J Comput Assist Tomogr* 1980;4:819–826.
39. Hoffman EJ, Huang S, Phelps ME, Kuhl DE. Quantitation in positron emission computed tomography: 4. Effect of accidental coincidences. *J Comput Assist Tomogr* 1981;5:391–400.
40. Jaszczak RJ, Greer KL, Floyd CE, Harris CC, Coleman RE. Improved SPECT quantification using compensation for scattered photons. *J Nucl Med* 1984;25:893–900.
41. Msaki P, Axelsson B, Dahl CM, Larsson SA. Generalized scatter correction method in SPECT using point scatter distribution functions. *J Nucl Med* 1987;28:1861–1869.
42. Manglos SH, Jaszczak RJ, Floyd CE, Hahn LJ, Greer KL, Coleman RE. Nonisotropic attenuation in SPECT: phantom tests of quantitative effects and compensation techniques. *J Nucl Med* 1987;28:1584–1591.
43. Weber DA, Eckerman KF, Dillman LT, Ryman JC. *MIRD: radionuclide data and decay schemes*. New York: Society of Nuclear Medicine; 1989.